Check for updates

# Effect of precipitating agent, N2 gas, extract volume and pH on the magnetic properties of magnetite nanoparticles by green synthesis from aqueous pomegranate peel extract

Marzieh Dehghani, Behnam Hajipour-Verdom and
Parviz Abdolmaleki*

Department of Biophysics, Faculty of Biological Sciences, Tarbiat Modares University, Tehran, Iran

Superparamagnetic nanoparticles (SPMNPs) have attracted considerable attention in biomedicine, particularly magnetic hyperthermia for cancer treatment. However, the development of efficient and eco-friendly methods for synthesizing SPMNPs remains a challenge. This study reports on a green synthesis approach for SPMNPs using pomegranate peel extract as a stabilizing agent. The effects of various synthesis parameters, including the type of precipitating agent ($NH_3$ and $NaOH$), $N_2$ gas, extract volume, and pH, were systematically investigated with regard to the size, morphology, and magnetic properties of the nanoparticles. The results showed that reducing the volume of the extract increased the saturation magnetization of the nanoparticles. $N_2$ gas was found to be essential in preventing the oxidation of the nanoparticles. The type of precipitating agent also affected the size and magnetization of the nanoparticles, with $NaOH$ leading to the synthesis of SPMNPs with higher magnetization (~4 times) compared to $NH_3$. Additionally, nanoparticles synthesized at pH 10 exhibited higher magnetization than those synthesized at pH 8 and 12. In conclusion, the optimized synthesis conditions significantly affected the magnetization and stability of SPMNPs. These nanoparticles are suitable for use in magnetic nanofluid hyperthermia applications.

KEYWORDS

superparamagnetic nanoparticles, green synthesis, pomegranate peel extract, synthesis optimization, magnetic hyperthermia

# Introduction

Nanotechnology, which involves the study and manipulation of particles at the nanoscale, has revolutionized various fields, including biomedicine and industry (Khan et al., 2019; Lim et al., 2021). Among the diverse nanomaterials, magnetic nanoparticles, particularly superparamagnetic nanoparticles (SPMNPs), have gained significant attention due to their unique properties and wide-ranging applications (Shabatina et al., 2020; Chen et al., 2021). Their magnetic responsiveness allows for easy manipulation and separation, making them valuable for magnetic drug delivery, biosensing, and environmental remediation (Molaabasi et al., 2018; Shamsipur et al., 2019; Ashoori et al., 2023).

Superparamagnetic magnetite ($Fe_3O_4$) nanoparticles possess unique magnetic properties that make them highly suitable for various biomedical applications, particularly in magnetic hyperthermia (Kolen'ko et al., 2014). These properties include simple synthesis and characteristics, chemical stability, and biocompatibility (Xu and Sun, 2009). Moreover, the ability to generate heat under an alternating magnetic field (magnetic hyperthermia) enables their use in targeted cancer therapy (Ebrahimpour et al., 2021). Various factors contribute to heat generation, including the intensity and frequency of the applied magnetic field, nanoparticle concentration, size, shape, composition, and coating, as well as the viscosity of the medium and the synthesis method of the nanoparticles (Campos et al., 2015). Additionally, the synthesis method and conditions employed significantly influence the magnetic properties of these nanoparticles. Commonly employed techniques for magnetite nanoparticle synthesis include co-precipitation, sol-gel, microemulsion, thermal decomposition, and green synthesis (Campos et al., 2015; Rajan and Sahu, 2020).

Currently, magnetite nanoparticles can be synthesized by applying the green chemistry metrics. The goal of green chemistry is to design chemical products and processes that reduce or eliminate the use and production of hazardous substances. The green chemistry metrics include the following: 1- Preventing the creation of waste (prevention), 2- Maximizing the use of all reactants in creating the final product (atomic economy), 3- Minimizing toxicity for humans and the environment (less hazardous chemical syntheses), 4- Safer design of chemicals with proper performance (designing safer chemicals), 5- Using safer solvents and auxiliaries (safer solvents and auxiliaries), 6- Conducting reactions at ambient temperature and pressure (design for energy efficiency), 7- Use of renewable raw materials (use of renewable feedstocks), 8- Minimizing the use of unnecessary substances (blocking groups; protective groups) (reduce derivatives), 9- Using catalytic reagents instead of stoichiometric reagents (catalysis), 10- Synthesis of degradable products (design for degradation), 11- Controlling the reaction time and preventing the formation of dangerous substances (real-time analysis for pollution prevention), 12- Use of safer chemicals to minimize accidents (inherently safer chemistry for accident prevention) (Anastas et al., 2000).

Green synthesis methods for magnetite nanoparticles offer a promising approach over conventional synthesis techniques that utilize natural resources, such as plant extracts, as reducing and stabilizing agents (Dehghani and Ghadam, 2023). These methods provide environmentally friendly, non-toxic, cost-effective, and biocompatible nanoparticles with controlled properties, making them attractive for use in antimicrobial treatments, anti-cancer therapies, and other biomedical applications (Mustapha et al., 2022). Phytochemical compounds present in plant extracts play a crucial role in reducing metal ions to nanoparticles and stabilizing them. This process prevents agglomeration and ensures uniform size distribution (Venkataraman, 2022). A study by Sathishkumar et al. demonstrated the synthesis of magnetite nanoparticles using *Couroupita guianensis Aubl* fruit extract, highlighting their antimicrobial and anti-cancer properties. The nanoparticles exhibited a great antimicrobial effect against different human pathogens, indicating their potential as antimicrobial agents. Additionally, they showed a dose-dependent cytotoxic effect against human hepatocellular carcinoma cells (Sathishkumar et al., 2018). In the study conducted by Yousefi et al., magnetite nanoparticles were synthesized using *Garcinia mangostana* fruit peel extract, focusing on investigating their anti-cancer properties. They found that the magnetic nanofluids exhibited acceptable specific absorption rate (SAR) values and demonstrated thermosensitive performance during hyperthermia experiments (Yusefi et al., 2021).

The synthesis method and conditions play a significant role in determining the magnetic properties of nanoparticles (Hadadian et al., 2022). Several parameters can influence the magnetic properties of magnetite nanoparticles. These include temperature, pH, use of inert gases (such as $N_2$ or Ar), precipitating agent, and the type and volume of the extract (Sathishkumar et al., 2018). The use of gas during synthesis can have a notable impact on the magnetization of nanoparticles, the formation of crystal structures, and the distribution of particle sizes. However, some studies provide examples of the different outcomes observed when $N_2$ gas was not used in the synthesis of magnetite nanoparticles. Ba-Abbad et al. synthesized magnetite nanoparticles in nitrogen-free conditions, which had ferromagnetic properties (Ba-Abbad et al., 2022). In contrast, Etemadifar et al. and Dorniani et al. carried out similar syntheses without $N_2$ gas and obtained nanoparticles with superparamagnetic properties (Dorniani et al., 2012; Etemadifar et al., 2018). These variations in magnetic properties could be attributed to the differences in the experimental conditions, such as the synthesis method, precursor materials, and reaction parameters. These parameters can significantly influence the size, shape, crystallinity, and surface properties of the nanoparticles, which in turn affect their magnetic behavior.

In this study, pomegranate peel (PP) extract was used as a coating and stabilizing agent for magnetite nanoparticles. PP extract is rich in bioactive compounds, with phenolic compounds being among the most important. The main phenolic compounds among them are tannins, flavonoids, phenolic acids, gallic acid, ellagic acid, catechin, and punicalagin (Fischer et al., 2011). Iranian PP extract is rich in phenolic compounds. For example, Ghasemi et al., (2023) reported, punicalagin, catechin, ellagic acid, and gallic acid account for 76.7%, 14.9%, 3.3%, and 3.1% of the eight monophenols recognized in pomegranate peel, respectively. Flavonoids in PP extract, with their various functional groups, play a crucial role in reducing metal ions and converting them into nanoparticles (Ramesh et al., 2015). Additionally, this study aims to optimize the synthesis conditions for obtaining superparamagnetic magnetite nanoparticles using a green synthesis approach. We investigated the role of $N_2$ gas, type of precipitating agent, volume of the extract, and pH on the magnetic properties of the nanoparticles. The findings of this study advance the field of nanotechnology and pave the way for the development of new magnetic nanomaterials with improved performance and application in biomedical research, including magnetic nanofluid hyperthermia and targeted drug delivery.

# Materials and methods

## Chemical reagents

$FeCl_2.4H_2O$, $FeCl_3.6H_2O$ and NaOH were purchased from Merck (Germany). $NH_3$ and HCL were purchased from Sigma-

**FIGURE 1**
The preparation of pomegranate peel extract.

Aldrich (Germany). Sweet pomegranate fruit was obtained from the orchards in Tehran province, Iran.

## Preparation of pomegranate peel extract

Fresh pomegranates were collected, de-seeded, and subsequently, the peel was carefully washed and cut into uniform pieces. The pomegranate peel (PP) dried for 2 weeks in the shade at 25°C to remove moisture and preserve its bioactive compounds. The dried PP was then ground into a fine powder using a home mill. To prepare the extract, 200 mg of the dry PP powder was added to 20 mL of distilled water in a heat-resistant container. The mixture was heated to 100°C to facilitate the extraction of bioactive compounds from the PP and then transferred to a water bath set at 90°C for 20 min. After cooling to room temperature, the extract was centrifuged at 4,000 rpm for 20 min. The supernatant was carefully collected and passed through a 0.2 μm filter. The final PP extract was stored in a refrigerator at 4°C to maintain its potency and prevent degradation (Figure 1).

## Synthesis and optimization of magnetite nanoparticles

To achieve superparamagnetic magnetite nanoparticles, the synthesis conditions were meticulously optimized. Initially, $FeCL_2$ (1 mM) was stirred for 5 min, with the option of utilizing $N_2$ gas. Subsequently, $FeCL_3$ (2 mM) was added to the solution, and stirring continued for an additional 20 min. During the nucleation phase, the pH was adjusted to 10 using either NaOH at room temperature or $NH_3$ at 60°C. Following the pH adjustment, the solution was stirred for an additional 20 min of stirring. The reaction then proceeded with or without the addition of 20 mL of PP extract (10 mg/mL) for 20 min. Subsequently, the samples were centrifuged at 4,000 rpm for 20 min. The resulting precipitate was washed thrice with distilled water and dried at 50°C for 4 h. Eight groups of synthesized magnetite nanoparticles were subjected to the necessary analyses. The synthesis steps and conditions are shown in Figures 2A–H; Table 1. Subsequently, the group exhibiting the most desirable superparamagnetic properties was selected, and its synthesis conditions were further optimized. The volume of the extract was investigated, considering 5 mL and 10 mL. The optimization steps and conditions for different extract volumes are illustrated in Figures

2I, J; Table 2. Additionally, pH values of 8 and 12 were evaluated for further pH optimization using NaOH. The steps and conditions involved in the pH optimization process are presented in Figures 2K, L; Table 3. Finally, the optimized sample underwent further analysis.

## Structural characterization of magnetite nanoparticles

The optical properties of magnetite nanoparticles were investigated using a spectrophotometer (PerkinElmer Inc., Waltham, MA, United States) in the wavelength range of 200–800 nm. The surface plasmon resonance (SPR) band and UV/Vis absorption were assessed to gain insights into the optical behavior of the nanoparticles. Dynamic light scattering (DLS) and zeta potential measurements were performed using a Zetasizer Nano ZS (Malvern Instruments Ltd., United Kingdom) to determine the particle size distribution and surface charge, respectively. Magnetic properties were studied using a vibrating sample magnetometer (VSM) manufactured by Daghigh Kavir Engineering Company (Iran). Hysteresis curves were obtained at room temperature to calculate parameters such as coercivity (HC), saturation magnetization (MS), and magnetic susceptibility permeability. Fourier-transform infrared spectroscopy (FTIR) analysis was carried out using a TENSOR 27 spectrophotometer (Bruker Optik GmbH, Germany) in the wavelength range of 400 to 4,000 cm$^{-1}$. This analysis provided information about the functional groups present on the surface of the nanoparticles (Kazemi-Ashtiyani et al., 2022). X-Ray diffraction (XRD) analysis was performed using an XRD Philips PW1730 (Netherlands) to investigate the crystal structure, grain size, interatomic distances, lattice parameters, and crystal defects of the nanoparticles. Field emission scanning electron microscope (FESEM) analysis was conducted using a FESEM ZEISS Sigma 300 (Germany) to obtain high-resolution images of the nanoparticles. Energy dispersive X-ray (EDAX) analysis was performed using the same FESEM instrument to identify the elemental composition and determine the weight or atomic percentage of each element present in the nanoparticles.

## Results and discussion

The use of green chemistry principles in the synthesis of nanomaterials has gained popularity in recent years (Mubayi

**FIGURE 2**
The synthesis of superparamagnetic magnetite nanoparticles was optimized through various conditions. Two different options for adjusting the pH were utilized: NaOH at room temperature and $NH_3$ at 60°C under different conditions of **(A, E)** control (without Pomegranate peel (PP) extract and $N_2$ gas), **(B, F)** with 20 mL PP extract (without $N_2$ gas), **(C, G)** with $N_2$ (without PP extract) and **(D, H)** with 20 mL PP extract/$N_2$ at pH 10, respectively. The volume of PP extract was conducted using **(I)** 5 mL and **(J)** 10 mL in presence of NaOH and $N_2$ gas at pH 10. The pH levels were optimized with 5 mL PP extract/$N_2$ at different **(K)** pH 8 and **(L)** pH 12 in presence of NaOH.

et al., 2012). Moreover, Metal and metal oxide nanoparticles, including magnetite nanoparticles, have attracted significant attention due to their unique properties such as optical, catalytic, magnetic, and electrical characteristics (Sengupta and Sarkar, 2015; Zare-Moghadam et al., 2020). Magnetite nanoparticles have found diverse applications in catalysis, sensors, drug delivery, MRI, and magnetic hyperthermia (Laurent et al., 2008). Achieving superparamagnetic properties in magnetite nanoparticles is crucial for applications such as magnetic hyperthermia. Superparamagnetic magnetite nanoparticles possess a strong magnetic moment in the presence of an external magnetic field, but lose their

magnetization once the field is removed. This property enables them to generate heat under an alternating magnetic field, which can be utilized for targeted cancer cell destruction in magnetic hyperthermia therapy. The challenge lies in synthesizing magnetite nanoparticles with superparamagnetic properties. However, by modifying the synthesis method and optimizing the relevant parameters, it is possible to obtain magnetite nanoparticles with the desired properties. This study aims to synthesize magnetite nanoparticles using green synthesis methods and optimize the synthesis conditions to achieve superparamagnetic properties suitable for magnetic hyperthermia. Eight different protocols were employed,

TABLE 1 Different conditions for synthesis of superparamagnetic magnetite nanoparticles using pomegranate peel (PP) extract with two different participating agents (NaOH and NH$_3$) in presence and absence of N$_2$ gas.

| Samples | Precipitating agent (pH 10) | | Iron source | N$_2$ gas | PP extract solution (20 mL) |
|---|---|---|---|---|---|
| | NaOH | NH$_3$ | | | |
| Control | ✓ | | FeCL$_2$+FeCL$_3$ (1:2) | | |
| With extract | ✓ | | FeCL$_2$+FeCL$_3$ (1:2) | | ✓ |
| With N$_2$ | ✓ | | FeCL$_2$+FeCL$_3$ (1:2) | ✓ | |
| With extract/N$_2$ | ✓ | | FeCL$_2$+FeCL$_3$ (1:2) | ✓ | ✓ |
| Control | | ✓ | FeCL$_2$+FeCL$_3$ (1:2) | | |
| With extract | | ✓ | FeCL$_2$+FeCL$_3$ (1:2) | | ✓ |
| With N$_2$ | | ✓ | FeCL$_2$+FeCL$_3$ (1:2) | ✓ | |
| With extract/N$_2$ | | ✓ | FeCL$_2$+FeCL$_3$ (1:2) | ✓ | ✓ |

TABLE 2 Optimizing the volume of pomegranate peel (PP) extract for synthesis of superparamagnetic magnetite nanoparticles in presence of NaOH, N$_2$ gas and different volume of 5 and 10 mL at pH 10.

| Sample | Precipitating agent | Iron source | N$_2$ gas | pH | Volume of PP extract (mL) |
|---|---|---|---|---|---|
| With extract/N$_2$ | NaOH | FeCL$_2$+FeCL$_3$ (1:2) | ✓ | 10 | 5 |
| With extract/N$_2$ | NaOH | FeCL$_2$+FeCL$_3$ (1:2) | ✓ | 10 | 10 |

TABLE 3 Optimization the pH level for synthesis of superparamagnetic magnetite nanoparticles in presence of NaOH, N$_2$ gas and 5 mL pomegranate peel (PP) extract at different pH 8, 10 and 12.

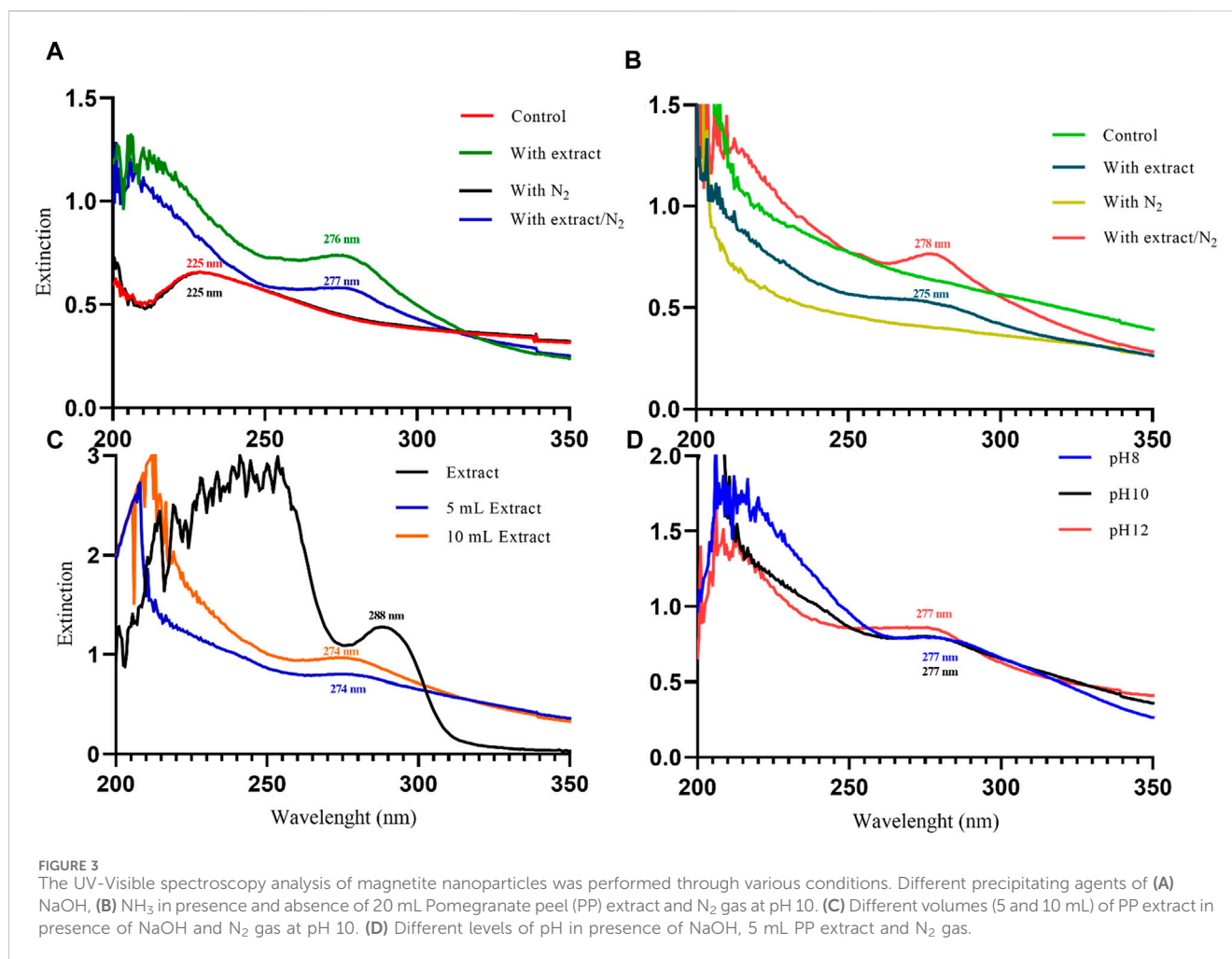| Sample | Precipitating agent | Iron source | N$_2$ gas | pH | Volume of PP extract (mL) |
|---|---|---|---|---|---|
| With extract/N$_2$ | NaOH | FeCL$_2$+FeCL$_3$ (1:2) | ✓ | 8 | 5 |
| With extract/N$_2$ | NaOH | FeCL$_2$+FeCL$_3$ (1:2) | ✓ | 10 | 5 |
| With extract/N$_2$ | NaOH | FeCL$_2$+FeCL$_3$ (1:2) | ✓ | 12 | 5 |

involving variations in the precipitating agent (NaOH and NH$_3$), the use of N$_2$ gas, the volume of PP extract, and the pH of the reaction (Figure 2; Table 1).

## UV-Vis analysis confirms the synthesis of magnetite nanoparticles

UV-Vis spectrophotometry was performed on the suspension containing nanoparticles to confirm their synthesis. This analysis allows us to observe the surface plasmon resonance (SPR) band of the nanoparticles, which is a manifestation of the interaction between the conduction electrons of the nanoparticles and incident photons. The SPR band is sensitive to the size and shape of the nanoparticles, as well as the dielectric constant of the surrounding medium (Jana et al., 2016). In a study conducted by Akanda et al., (2023) in 2023, magnetite nanoparticles synthesized with *Tamarindus indica* leaf extract exhibited an SPR band at 280 nm. Similarly, Kiwumulo et al.,2022 synthesized magnetite nanoparticles using *Moringa oleifera* extract in 2022, which displayed a strong SPR band at 300 nm. In 2020, Azizi

synthesized magnetite nanoparticles using tea extract, resulting in a wide SPR band ranging from 500 to 700 nm in the visible range (Azizi, 2020). In this study, magnetite nanoparticles synthesized using different protocols exhibited SPR bands in the UV range. Initially, when NaOH was used as the precipitating agent, the samples without extract (control and with N$_2$) showed an SPR band at 225 nm. However, with the addition of 20 mL of PP extract, the SPR band showed a red shift to 276 nm (with extract) and 277 nm (with extract/N$_2$). Indeed, with the increasing size of nanoparticles, the SPR band shows a red shift (Huang and El-Sayed, 2010). This indicates that the PP extract increased the size of the magnetite nanoparticles (Figure 3A).

In contrast, when NH$_3$ was used as the precipitating agent, the samples without extract did not exhibit a clear SPR band. However, the samples containing the extract showed SPR bands at 275 nm (with extract) and 278 nm (with extract/N$_2$) (Figure 3B). The observed red shift of the SPR band with increasing nanoparticle size is consistent with the literature. For particles larger than 100 nm, the SPR band broadening is also evident due to the dominant contributions from higher-order electron oscillations (Huang and El-Sayed, 2010). Overall, the UV-Vis analysis confirms the

**FIGURE 3**
The UV-Visible spectroscopy analysis of magnetite nanoparticles was performed through various conditions. Different precipitating agents of **(A)** NaOH, **(B)** $NH_3$ in presence and absence of 20 mL Pomegranate peel (PP) extract and $N_2$ gas at pH 10. **(C)** Different volumes (5 and 10 mL) of PP extract in presence of NaOH and $N_2$ gas at pH 10. **(D)** Different levels of pH in presence of NaOH, 5 mL PP extract and $N_2$ gas.

successful synthesis of magnetite nanoparticles and provides insights into the influence of synthesis conditions on their size and optical properties.

## Hydrodynamic diameter of magnetite nanoparticles

DLS analysis was performed to compare the hydrodynamic diameter of the synthesized nanoparticles. The hydrodynamic diameter refers to the size of the particles along with the "electrical double layer" formed by solvent molecules surrounding them. DLS relies on the Brownian motion of dispersed particles, where smaller particles exhibit rapid movements while larger particles display slower motion (Maguire et al., 2018). The results obtained from both UV-Vis spectroscopy and DLS analysis are in complete agreement. Samples containing PP extract demonstrated a larger hydrodynamic diameter, indicating that they are larger compared to the other groups. Indeed, the synthesis of nanoparticles includes three steps: nucleation, growth, and coating. If the aqueous extract of PP is added during the nucleation or growth stage. This behavior can be attributed to the role of PP extract in reducing iron ions, which leads to faster

nucleation and faster growth of nanoparticles. But in this research, nucleation and growth were done, and then PP extract was added as a coating and stabilizing agent. Therefore, the larger size of the nanoparticles is due to the presence of functional groups of the extract on the surface of the magnetite nanoparticles (Skandalis et al., 2017).

The hydrodynamic diameter of the synthesized nanoparticles across the eight different protocols is summarized in Table 4. Additionally, Figures 4A–H presents the size distribution diagrams for the magnetite nanoparticles. For biomedical applications, the range of hydrodynamic diameter for nanoparticles should generally be less than 250 nm (Islam et al., 2020). All the synthesized magnetite nanoparticles met this criterion, indicating their potential suitability for biomedical applications.

## Surface charge of magnetite nanoparticles

Zeta potential analysis was performed to evaluate the surface charge of the synthesized nanoparticles. The zeta potential provides information about the surface charge of nanoparticles, which plays a crucial role in their long-term stability. The presence of surface

**TABLE 4** The hydrodynamic diameter of synthesized superparamagnetic magnetite nanoparticles in the presence and absence of $N_2$ gas and 20 mL pomegranate peel extract using two participating agents of NaOH and $NH_3$ at pH 10.

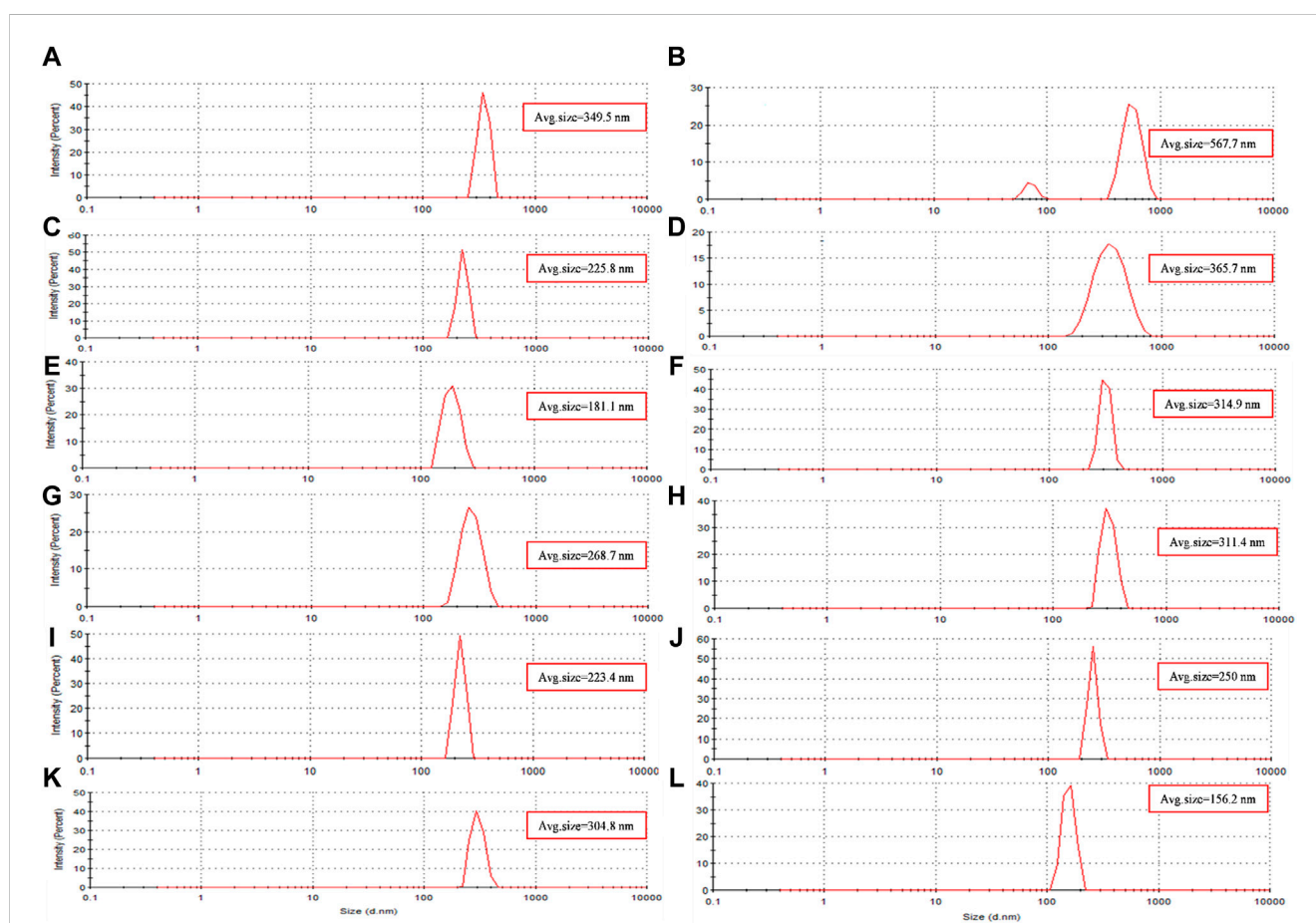| Sample | Precipitating agent (pH 10) | | Hydrodynamic diameter (nm) |
|---|---|---|---|
| | NaOH | $NH_3$ | |
| Control | ✓ | | 349.5 |
| With extract | ✓ | | 567.7 |
| With $N_2$ | ✓ | | 225.8 |
| With extract/$N_2$ | ✓ | | 365.7 |
| Control | | ✓ | 188.1 |
| With extract | | ✓ | 314.9 |
| With $N_2$ | | ✓ | 268.7 |
| With extract/$N_2$ | | ✓ | 311.4 |



**FIGURE 4**
The size distribution diagram of synthesized magnetite nanoparticles was analyzed through various conditions. Two different precipitating agents of NaOH at room temperature and $NH_3$ at 60°C under different conditions of **(A, E)** control (without Pomegranate peel (PP) extract and $N_2$ gas), **(B, F)** with 20 mL PP extract (without $N_2$ gas), **(C, G)** with $N_2$ (without PP extract) and **(D, H)** with 20 mL PP extract/$N_2$ at pH 10, respectively. Different volumes of PP extract at **(I)** 5 mL and **(J)** 10 mL in presence of NaOH and $N_2$ gas at pH 10. pH levels at **(K)** pH 8 and **(L)** pH 12 in presence of NaOH and 5 mL PP extract/$N_2$ gas.

charge on particles is the primary factor contributing to the stability of colloidal systems. When nanoparticles have similarly charged surfaces, they repel each other, preventing agglomeration or aggregation (Doymuş, 2007). Many factors such as the size of nanoparticles, the nature of the solution, ionic strength, concentration of dispersion, pH, buffer type, density,
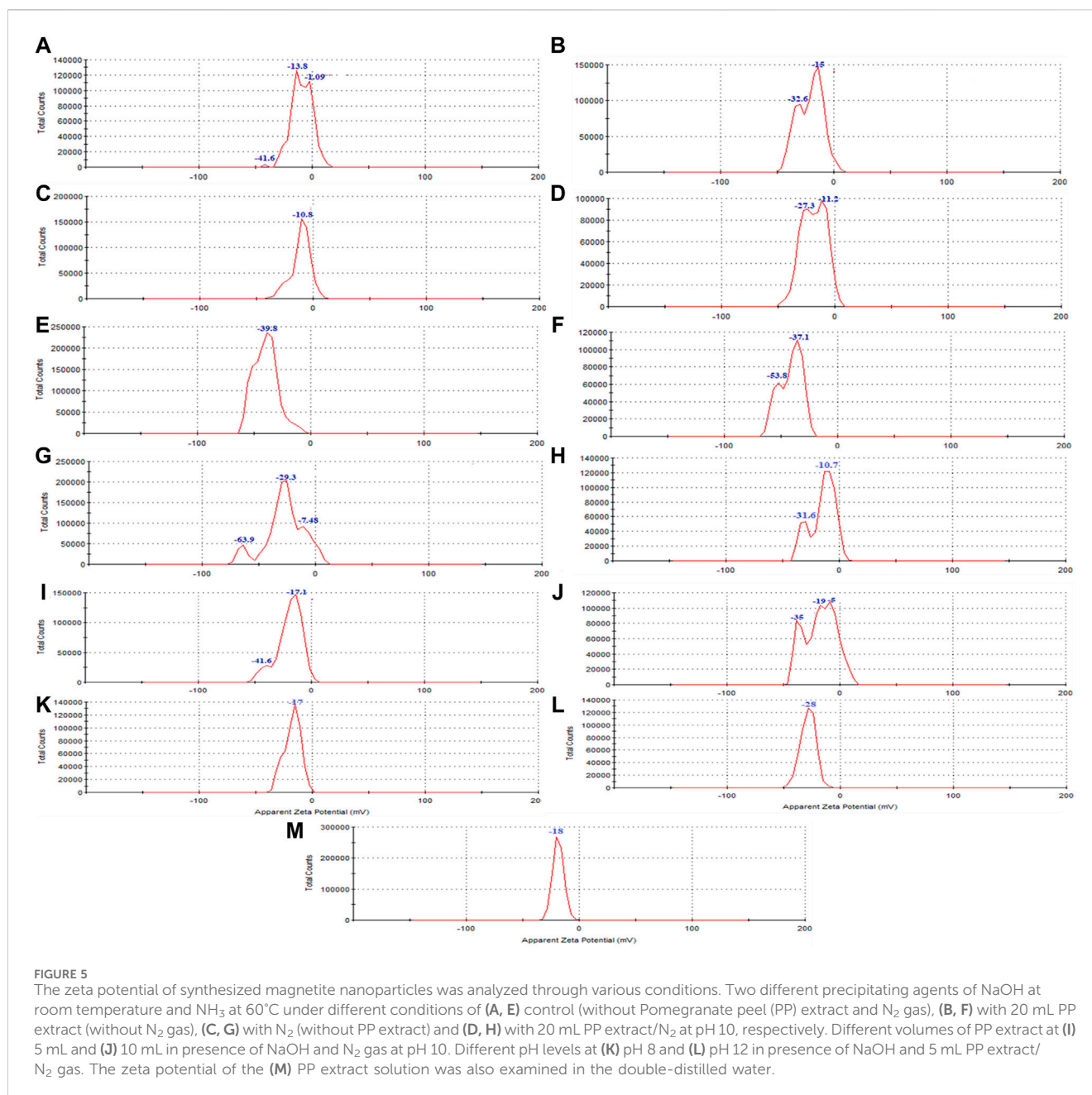
**FIGURE 5**
The zeta potential of synthesized magnetite nanoparticles was analyzed through various conditions. Two different precipitating agents of NaOH at room temperature and $NH_3$ at 60°C under different conditions of **(A, E)** control (without Pomegranate peel (PP) extract and $N_2$ gas), **(B, F)** with 20 mL PP extract (without $N_2$ gas), **(C, G)** with $N_2$ (without PP extract) and **(D, H)** with 20 mL PP extract/$N_2$ at pH 10, respectively. Different volumes of PP extract at **(I)** 5 mL and **(J)** 10 mL in presence of NaOH and $N_2$ gas at pH 10. Different pH levels at **(K)** pH 8 and **(L)** pH 12 in presence of NaOH and 5 mL PP extract/ $N_2$ gas. The zeta potential of the **(M)** PP extract solution was also examined in the double-distilled water.

temperature, pressure, and formulation method such as the use of ultrasound affect the zeta potential (Kirby and Hasselbrink, 2004). The change in pH, Precipitating agent, temperature, and the volume of PP extract causes a change in the size of magnetite nanoparticles, which causes a change in the electric charge density on the surface of magnetite nanoparticles and as a result, increases the repulsive forces between them (Khairul et al., 2016).
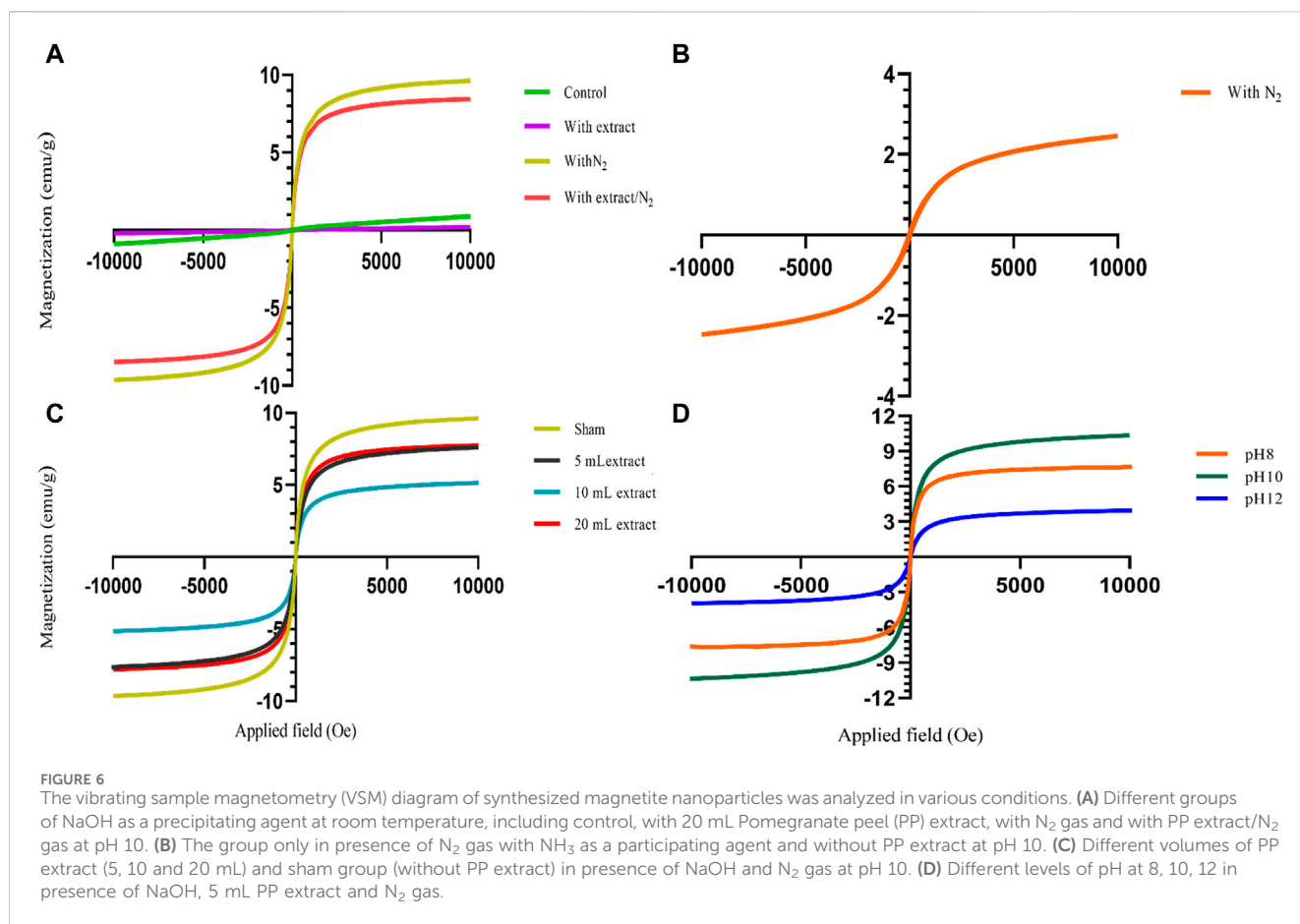
The Zeta potential diagram and the charge distribution of the extract (Figure 5M) and magnetite nanoparticles are shown in (Figures 5A–H). The results indicate that the extract and all the samples of synthesized nanoparticles exhibited a negative zeta potential. A negative zeta potential suggests that the surfaces of the nanoparticles carry a net negative charge. This negative charge contributes to the electrostatic repulsion between

particles, leading to their stability and preventing their aggregation or clumping.

## Magnetic properties of magnetite nanoparticles

The presence of different agents during the synthesis of nanoparticles can significantly impact their magnetic properties. As shown in Figures 2E–H, the use of $NH_3$ as the precipitating agent resulted in nanoparticles that did not exhibit significant magnetic properties, while the use of NaOH, particularly in the presence of $N_2$ gas, led to the acquisition of magnetic properties by the nanoparticles (Figures 2C, D). Because increasing the

**FIGURE 6**
The vibrating sample magnetometry (VSM) diagram of synthesized magnetite nanoparticles was analyzed in various conditions. **(A)** Different groups of NaOH as a precipitating agent at room temperature, including control, with 20 mL Pomegranate peel (PP) extract, with $N_2$ gas and with PP extract/$N_2$ gas at pH 10. **(B)** The group only in presence of $N_2$ gas with $NH_3$ as a participating agent and without PP extract at pH 10. **(C)** Different volumes of PP extract (5, 10 and 20 mL) and sham group (without PP extract) in presence of NaOH and $N_2$ gas at pH 10. **(D)** Different levels of pH at 8, 10, 12 in presence of NaOH, 5 mL PP extract and $N_2$ gas.
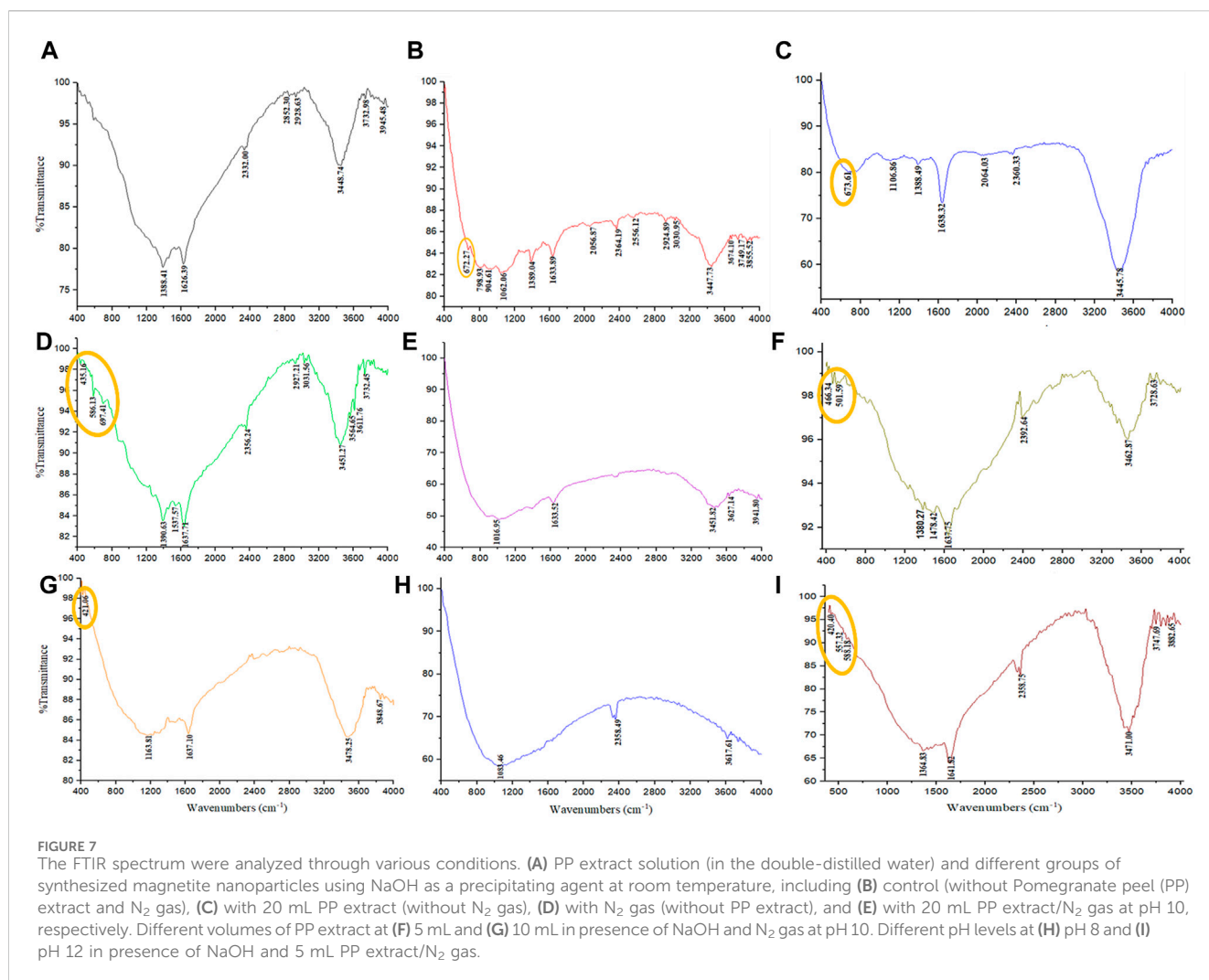
temperature affects the saturation magnetization of nanoparticles. Using $NH_3$ as a precipitating agent at 60°C; decreased the saturation magnetization of magnetite nanoparticles. However, when NaOH was used as a precipitation agent at room temperature; the saturation magnetization of nanoparticles increased (Nkurikiyimfura et al., 2020). Presence of an external magnetic field can induce a strong magnetic moment in superparamagnetic nanoparticles, but they lose their magnetization when the field is removed, which is a desirable property for magnetic fluid hyperthermia applications. Moreover, VSM analysis provides information about the magnetic moment, saturation magnetization, and coercivity of the nanoparticles. The VSM analysis revealed that the nanoparticles synthesized under $N_2$ gas exhibited superparamagnetic properties. On the other hand, the samples that were not synthesized under $N_2$ gas demonstrated diamagnetic properties and were deemed unsuitable for magnetic fluid hyperthermia (Figures 6A, B). The formation of a non-magnetic layer such as extract on the surface of the nanoparticles decreased the magnetization of the nanoparticles, kwon as a dead magnetic layer (Elizondo-Villarreal et al., 2022). The saturation magnetization for the particles in presence of $N_2$ gas was 10 emu/g, while in presence of extract/$N_2$ gas was 7 emu/g. The results provide insights that the magnetic properties of magnetite nanoparticles are strongly influenced by their size and the presence of different agents during synthesis. The use of VSM and other characterization techniques is vital for understanding the behavior of these nanoparticles in different environments and their potential applications.

## Functional groups of extract and magnetite nanoparticles

FTIR analysis was performed to identify the functional groups present in the PP extract and the magnetite nanoparticles. FTIR spectroscopy provides information about the chemical bonding and molecular structure of materials. The FTIR spectra of the PP extract and nanoparticles are shown in Figures 7A–E. The main peaks of the FTIR spectra are summarized in Table 5. The FTIR spectrum of the extract shows peaks at 3,945.48, 3,732.98, 3,448.74 $cm^{-1}$ (O-H stretching), 2,928.63 and 2,852.30 $cm^{-1}$ (C-H stretching), 1,626.39 $cm^{-1}$ (C=O stretching), 1,388.41 $cm^{-1}$ (C-H bending), and 2,332.00 $cm^{-1}$ (C-O bending). These peaks indicate the presence of various functional groups, including hydroxyl, carbonyl, and alkene groups. For the magnetite nanoparticles synthesized with NaOH, the FTIR spectrum reveals a peak at 672.27 $cm^{-1}$ (Fe-O stretching). However, when nanoparticles synthesized solely with NaOH and $N_2$ gas, peaks are observed at 435.16 $cm^{-1}$ (Fe-O stretching), 586.13 $cm^{-1}$ (Fe-O stretching), and 697.41 $cm^{-1}$ (Fe-O stretching). These peaks confirm the presence of iron oxide (magnetite) in the nanoparticles. The FTIR spectrum of the magnetite nanoparticles synthesized with NaOH and PP extract

**FIGURE 7**
The FTIR spectrum were analyzed through various conditions. **(A)** PP extract solution (in the double-distilled water) and different groups of synthesized magnetite nanoparticles using NaOH as a precipitating agent at room temperature, including **(B)** control (without Pomegranate peel (PP) extract and $N_2$ gas), **(C)** with 20 mL PP extract (without $N_2$ gas), **(D)** with $N_2$ gas (without PP extract), and **(E)** with 20 mL PP extract/$N_2$ gas at pH 10, respectively. Different volumes of PP extract at **(F)** 5 mL and **(G)** 10 mL in presence of NaOH and $N_2$ gas at pH 10. Different pH levels at **(H)** pH 8 and **(I)** pH 12 in presence of NaOH and 5 mL PP extract/$N_2$ gas.

shows a peak at 673.61 cm$^{-1}$ (Fe-O stretching), slightly shifted compared to the peak observed for the nanoparticles synthesized without extract. This shift may be due to the interaction between the extract and the magnetite nanoparticles. Notably, in the FTIR spectrum of the magnetite nanoparticles synthesized with NaOH, PP extract, and $N_2$ gas does not show any Fe-O peaks.

## Optimization of extract volume for magnetite nanoparticle synthesis

After performing a series of characterization analyses, including UV-Vis, DLS, zeta potential, VSM, and FTIR, it was determined that the extract/$N_2$ condition was the best group for further optimization. To optimize the volume of PP extract used in the synthesis, two additional volumes 5 and 10 mL of extract were investigated (Table 2). The nanoparticles synthesized with these different extract volumes were characterized, and the results were used to determine the optimal extract volume for synthesizing superparamagnetic magnetite nanoparticles with the desired magnetic properties.

The results of UV-Vis and DLS analyses provide insights into the effect of PP extract volume on the size of the magnetite nanoparticles. Both the nanoparticles synthesized with 5 mL and 10 mL of extract exhibit a SPR band at 274 nm in the UV-Vis spectra. This SPR band is blue-shifted compared to the peak observed for the PP extract at 288 nm (Figure 3C). The blue shift indicates a decrease in the size of the nanoparticles. This observation is confirmed by the DLS analysis, where the hydrodynamic diameter of the nanoparticles synthesized with 5 mL of extract is 223 nm, while that of the nanoparticles synthesized with 10 mL of extract is 250 nm (Figures 4I, J). Thus, increasing the volume of extract leads to an increase in the size of the nanoparticles. These findings suggest that the volume of PP extract plays a crucial role in controlling the size of the synthesized magnetite nanoparticles.

The zeta potential analysis shows indicates that both magnetite nanoparticles synthesized with 5 mL and 10 mL of extract possess a negative zeta potential, indicating a negative surface charge and contributing to their stability in aqueous solutions (Figures 5I, J). The synthesized nanoparticles with both extract volumes also exhibit magnetic behavior, as they are attracted by magnets (Figures 2I, J). VSM analysis confirms that both samples display superparamagnetic properties, meaning they possess a strong magnetic moment in the presence of an external magnetic field but lose their magnetization when the field is removed. However, the

TABLE 5 The FTIR spectrum were analyzed the pomegranate peel (PP) extract solution (in the double-distilled water) and different groups of synthesized superparamagnetic magnetite nanoparticles using NaOH as a precipitating agent, including control, with 20 mL PP extract, with $N_2$ gas, and with 20 mL PP extract/$N_2$ gas at pH 10.

| Samples | Wave number (cm$^{-1}$) | Band assignment | References |
|---|---|---|---|
| PP extract | 3,945.48 | O–H stretching | Kumar et al. (2014) |
| | 3,732.98 | O–H stretching | Kumar et al. (2014) |
| | 3,448.74 | O–H stretching | Kumar et al. (2014) |
| | 2,928.63 | C-H stretching | Kumar et al. (2014) |
| | 2,852.30 | C-H stretching | Kumar et al. (2014) |
| | 2,332.00 | C-O bending | Mishra et al. (2014) |
| | 1,626.39 | C=O stretching | Akshay et al. (2020) |
| | 1,388.41 | C-H bending | Trivedi et al. (2015) |
| Control | 3,855.52 | O-H stretching | Kumar et al. (2014) |
| | 3,749.17 | O-H stretching | Kumar et al. (2014) |
| | 3,674.10 | O-H stretching | Kumar et al. (2014) |
| | 3,447.73 | O-H stretching | Kumar et al. (2014) |
| | 3,030.95 | C-H stretching | Matrajt et al. (2004) |
| | 2,924.89 | C-H stretching | Kumar et al. (2014) |
| | 2,556.12 | S-H bending | Hakami et al. (2012) |
| | 2,364.19 | O=C=O stretching | Harris et al. (2002) |
| | 2056.87 | C=O stretching | Hakami et al. (2012) |
| | 1,633.89 | C=C stretching | Nandiyanto et al. (2016) |
| | 1,389.04 | C-H bending | Harris et al. (2002) |
| | 1,062.06 | C-O stretching | Buazar et al. (2016) |
| | 904.61 | C=C bending | Harris et al. (2002) |
| | 798.93 | C=C bending | Harris et al. (2002) |
| | 672.27 | Fe–O bonding | Buazar et al. (2016), Akshay et al. (2020) |
| With PP extract | 3,445.78 | O-H stretching | Kumar et al. (2014) |
| | 2,360.33 | O=C=O stretching | Harris et al. (2002) |
| | 2064.03 | C=C=N stretching | Hakami et al. (2012) |
| | 1,638.32 | C=C stretching | Nandiyanto et al. (2016) |
| | 1,388.49 | C-H bending | Harris et al. (2002) |
| | 1,106.86 | C-N stretching | Akshay et al. (2020) |
| | 673.61 | Fe–O bonding | Akshay et al. (2020) |
| With $N_2$ | 3,732.45 | O-H stretching | Kumar et al. (2014) |
| | 3,611.76 | O-H stretching | Kumar et al. (2014) |
| | 3,564.65 | O-H stretching | Kumar et al. (2014) |
| | 3,451.27 | O-H stretching | Kumar et al. (2014) |
| | 3,031.56 | C-H stretching | Matrajt et al. (2004) |
| | 2,927.21 | C-H stretching | Kumar et al. (2014) |
| | 2,356.24 | O=C=O stretching | Harris et al. (2002) |

(Continued on following page)

TABLE 5 (*Continued*) The FTIR spectrum were analyzed the pomegranate peel (PP) extract solution (in the double-distilled water) and different groups of synthesized superparamagnetic magnetite nanoparticles using NaOH as a precipitating agent, including control, with 20 mL PP extract, with $N_2$ gas, and with 20 mL PP extract/$N_2$ gas at pH 10.

| Samples | Wave number (cm$^{-1}$) | Band assignment | References |
|---|---|---|---|
| | 1,637.71 | C=C stretching | Nandiyanto et al. (2016) |
| | 1,537.57 | N-O stretching | Harris et al. (2002) |
| | 1,390.63 | C-H bending | Harris et al. (2002) |
| | 697.41 | Fe–O bonding | Akshay et al. (2020) |
| | 586.13 | Fe–O bonding | Buazar et al. (2016) |
| | 435.16 | Fe–O bonding | Mazrouaa et al. (2019) |
| with PP extract/$N_2$ | 3,941.80 | O-H stretching | Kumar et al. (2014) |
| | 3,627.14 | O-H stretching | Kumar et al. (2014) |
| | 3,451.82 | O-H stretching | Kumar et al. (2014) |
| | 1,633.52 | C=O stretching | Akshay et al. (2020) |
| | 1,016.95 | C-N stretching | Buazar et al. (2016) |

TABLE 6 The FTIR analysis of synthesized superparamagnetic magnetite nanoparticles in presence of $N_2$ gas and different pomegranate peel (PP) extract volume 5 and 10 mL using NaOH as participating agents at pH 10.

| PP extract volume | Wave number (cm$^{-1}$) | Band assignment | References |
|---|---|---|---|
| 5 mL | 3,728.63 | O-H stretching | Kumar et al. (2014) |
| | 3,462.87 | O-H stretching | Kumar et al. (2014) |
| | 2,392.64 | O=C=O stretching | Harris et al. (2002) |
| | 1,637.75 | C=C stretching | Nandiyanto et al. (2016) |
| | 1,478.42 | C-O bending | Harris et al. (2002) |
| | 1,380.27 | C-H bending | Harris et al. (2002) |
| | 501.59 | Fe–O bonding | Buazar et al. (2016) |
| | 466.34 | Fe–O bonding | Mazrouaa et al. (2019) |
| 10 mL | 3,848.67 | O-H stretching | Kumar et al. (2014) |
| | 3,478.25 | O-H stretching | Kumar et al. (2014) |
| | 1,637.10 | C=C stretching | Nandiyanto et al. (2016) |
| | 1,163.81 | C-N stretching | Harris et al. (2002) |
| | 421.06 | Fe–O bonding | Mazrouaa et al. (2019) |

nanoparticles synthesized with 5 mL of extract exhibit a higher magnetization compared to those synthesized with 10 mL of extract (Figure 6C). This difference in magnetization may be attributed to the smaller size of the nanoparticles synthesized with 5 mL of extract, as smaller nanoparticles have larger magnetic domains, leading to stronger interaction with the magnetic field.

The surface functional groups of the synthesized nanoparticles were characterized using FTER analysis. The FTIR spectra reveal the presence of a distinct Fe-O band (Figures 7F, G). The main peaks observed in the FTIR spectra are summarized in Table 6. Notably, the magnetite nanoparticles synthesized using 5 mL of extract volume exhibit Fe-O peaks at 466.34 and 501.59 cm$^{-1}$, while those synthesized with 10 mL of extract volume display a Fe-O peak at 421.06 cm$^{-1}$.

## Optimization of pH levels for magnetite nanoparticle synthesis

In the subsequent step, the magnetite nanoparticles synthesized using 5 mL of extract were selected based on their higher saturation magnetization and the presence of the Fe-O band. The pH of the synthesis process was then optimized by synthesizing nanoparticles at pH 8 and pH 12 (Table 3) to explore their magnetic susceptibility properties. Indeed, pH affects solubility. For ionic compounds containing basic anions, solubility is inversely proportional to pH. Solubility increases as the pH of the solution decreases. If the pH is higher than 3.5 the ferric iron ($Fe^{3+}$) will become insoluble and precipitate but ferrous iron ($Fe^{2+}$) precipitates at pH 8 (Balintova and Petrilakova, 2011).

TABLE 7 The FTIR analysis of synthesized superparamagnetic magnetite nanoparticles in presence of $N_2$ gas and 5 mL pomegranate peel extract using NaOH as participating agents at different pH 8 and 12.

| pH levels | Wave number (cm$^{-1}$) | Band assignment | References |
|---|---|---|---|
| pH 8 | 3,617.61 | O-H stretching | Kumar et al. (2014) |
| | 2,358.49 | C-O band | Mishra et al. (2014) |
| | 1,083.46 | C-O stretching | Buazar et al. (2016) |
| pH 12 | 3,882.65 | O-H stretching | Kumar et al. (2014) |
| | 3,747.69 | O-H stretching | Kumar et al. (2014) |
| | 3,471.00 | O-H stretching | Kumar et al. (2014) |
| | 2,358.75 | C-O banding | Mishra et al. (2014) |
| | 1,641.82 | C=O stretching | Akshay et al. (2020) |
| | 1,364.83 | C-H banding | Trivedi et al. (2015) |
| | 588.18 | Fe–O bonding | Buazar et al. (2016) |
| | 557.32 | Fe–O bonding | Buazar et al. (2016) |
| | 420.40 | Fe–O bonding | Mazrouaa et al. (2019) |
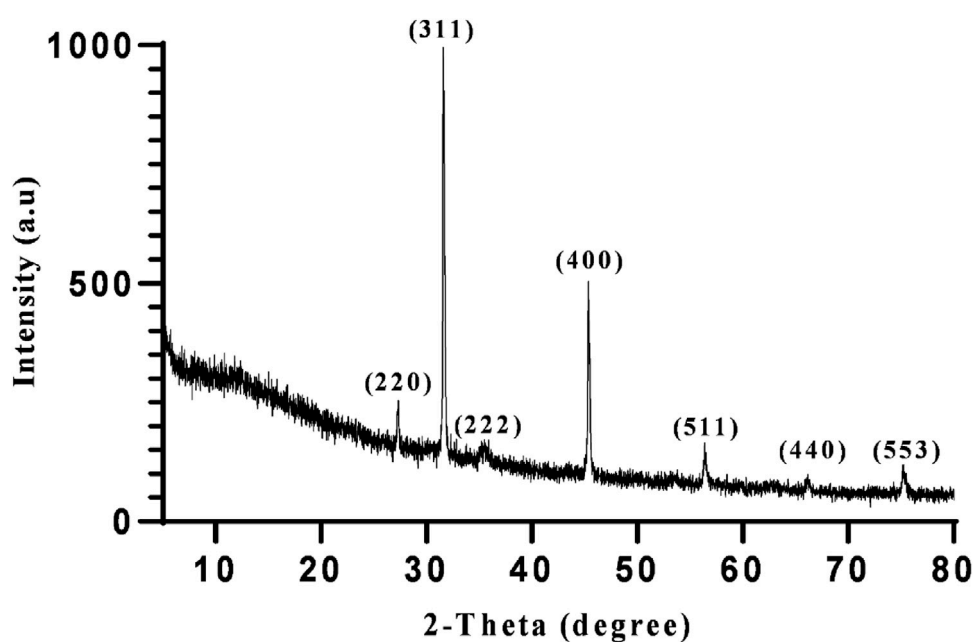


FIGURE 8
The XRD profile of synthesized superparamagnetic magnetite ($Fe_3O_4$) nanoparticles using NaOH with 5 mL Pomegranate peel extract in presence of $N_2$ gas at pH 10 as optimum conditions.

The results from UV-Vis analysis indicate that both the nanoparticles synthesized at pH 8 and pH 12 exhibit SPR peaks at 277 nm (Figure 3D). This suggests that the nanoparticles have similar optical properties regardless of the pH.

DLS analysis reveales that the hydrodynamic diameter of the nanoparticles synthesized at pH 12 is 156 nm, while that of the nanoparticles synthesized at pH 8 is 304.8 nm (Figure 4K, L). The larger hydrodynamic diameter at pH 8 indicates an increase in the size of the nanoparticles compared to those synthesized at pH 12.

Zeta potential analysis indicates that both the nanoparticles synthesized at pH 8 and pH 12 have a negative zeta potential. The nanoparticles synthesized at pH 8 have a zeta potential of −17.6 mV, while those synthesized at pH 12 have a zeta potential of −28 mV (Figures 5K, L). The negative zeta potential suggests that the nanoparticles have a negatively
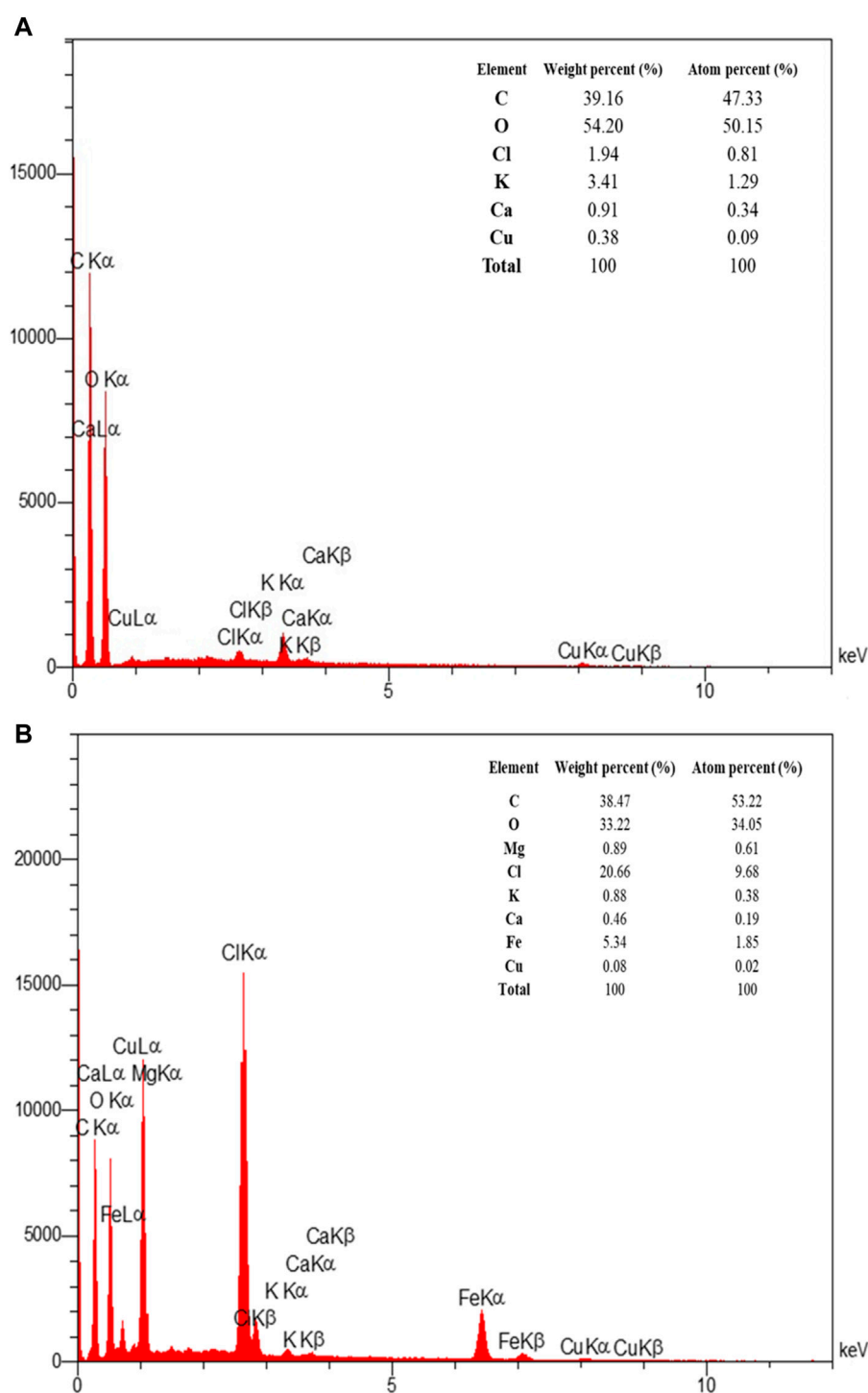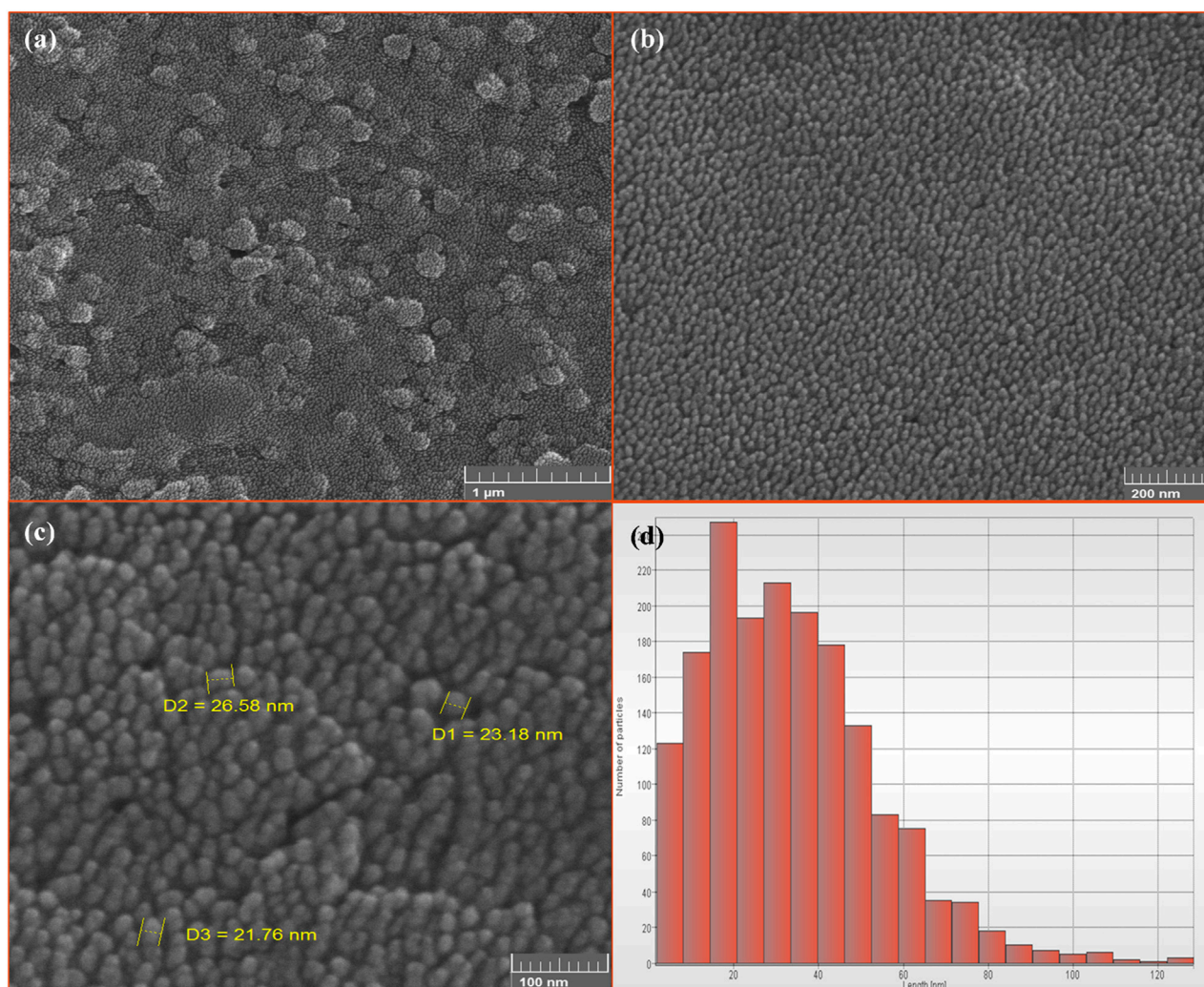
**FIGURE 9**
The EDAX spectra of **(A)** Pomegranate peel extract solution (in the double-distilled water) and **(B)** synthesized superparamagnetic magnetite ($Fe_3O_4$) nanoparticles using NaOH with 5 mL PP extract volume in presence of $N_2$ gas at pH 10 as optimum conditions.

charged surface, contributing to their stability in aqueous solutions.

FTIR analysis was conducted to evaluate the functional groups present on the surface of these nanoparticles. Notably, the nanoparticles synthesized at pH 8 did not exhibit the Fe-O band, whereas the Fe-O band was observed in the nanoparticles synthesized at pH 12 (Figures 7H, I). The presence of the Fe-O band confirms the formation of magnetite nanoparticles (Table 7).

VSM analysis indicates that all synthesized magnetite nanoparticles exhibit superparamagnetic behavior at pH 8, 10, and 12. However, the nanoparticles synthesized at pH 10 demonstrate a higher magnetization compared to the

**FIGURE 10**
The FE-SEM images of synthesized superparamagnetic magnetite ($Fe_3O_4$) nanoparticles using NaOH with 5 mL PP extract volume in presence of $N_2$ gas at pH 10 with different resolution. Scale bars: **(A)** 1 μm, **(B)** 200 nm and **(C)** 100 nm. **(D)** The size distribution of $Fe_3O_4$ nanoparticles.

other samples. Because in the range of pH 9.7 to 10.6, pure magnetite nanoparticles are synthesized. pH values below 8.5 lead to the formation of side-products to magnetite, specifically goethite and maghemite (Andrade et al., 2010) (Figure 6D).

Based on these findings, the optimal conditions for synthesizing magnetite nanoparticles include using NaOH as the participating agent, a 5 mL extract volume, conducting the synthesis under $N_2$ gas atmosphere, maintaining a pH of 10, and performing the reaction at room temperature. Under these conditions, the nanoparticles exhibit superparamagnetic properties and achieve a higher level of magnetization compared to other synthesis conditions. Identifying these optimal conditions is crucial as it enables researchers to determine the most favorable parameters for synthesizing magnetite nanoparticles with the desired magnetic properties. These SPMNPs with enhanced magnetization hold significant potential for various applications, including magnetic separation, biomedical diagnostics, and targeted drug delivery systems.

## More analysis of magnetite nanoparticles in the optimized synthesis conditions

In the following step, XRD, FESEM, and EDAX analysis were performed to fully characterize the optimized magnetite nanoparticles synthesized using 5 mL of extract at pH 10. XRD analysis was conducted to confirm the crystal structure and phase purity of the synthesized nanoparticles. As shown in Figure 8, the XRD patterns confirmed the synthesis of magnetite nanoparticles. The diffraction peaks observed in the XRD pattern correspond to specific crystallographic planes, such as 220, 311, 222, 400, 511, 440, and 533 (Silva et al., 2013). The presence of sharp peaks suggests a crystalline nature of the nanoparticles, while the presence of broad peaks indicates the presence of ultra-fine and small crystallite sizes (Medina-Zazueta et al., 2023).

EDAX analysis was used to determine the elemental composition of both the extract and the optimized magnetite nanoparticles. Figure 9 displays the EDAX spectrum of the

extract and magnetite nanoparticles. The analysis confirms that the magnetite nanoparticles synthesized under the optimized conditions contain compositions of iron and oxygen. This analysis provides quantitative information about the percentage of these elements present in the nanoparticles, verifying their elemental composition.

FESEM analysis results indicate that the synthesized magnetite nanoparticles are monodisperse and exhibit a spherical shape. Figure 10 provides visual evidence of the nanoparticles at different resolutions, showcasing their size distribution. The average size of the synthesized nanoparticles is approximately 25 nm, falling within the recommended range of 10–100 nm for nanoparticles used in magnetic nanofluid hyperthermia (Chang et al., 2018). Nanoparticles smaller than 10 nm are generally ineffective in heat generation. The monodispersity and superparamagnetic properties of the synthesized magnetite nanoparticles make them suitable for generating uniform and effective heat in magnetic nanofluid hyperthermia applications (Nguyen and Kim, 2016).

## Conclusion

The green synthesis of superparamagnetic magnetite nanoparticles using biological extracts has emerged as a highly attractive method, renowned for its safety, cost-effectiveness, and eco-friendliness. Various studies, including those utilizing different biological sources such as *Citrus sinensis* peel extract, *M. oleifera*, and *Eucalyptus globulus* extract, have demonstrated successful green synthesis (Andrade-Zavaleta et al., 2022; Kiwumulo et al., 2022; Eldeeb et al., 2023). In this study, we prioritized green chemistry metrics, employing the aqueous extract of PP as a stabilizer for magnetite nanoparticles. Notably, the synthesis occurred under ambient pressure, avoiding the generation of toxic waste, high temperatures, and hazardous solvents. Exploring the optimization of synthesis parameters, including the PP extract, $N_2$ gas, precipitating agents, and pH variations, showed crucial. Our research underscores the promise of this green synthesis method for diverse applications, notably in magnetic nanofluid hyperthermia and targeted drug delivery systems. The synthesized nanoparticles exhibit desirable characteristics such as biocompatibility, stability, and suitable magnetic properties, positioning them favorably for biomedical applications.

Optimized conditions, such as the presence of $N_2$ gas, NaOH as a precipitating agent, specific extract volumes, and pH levels, significantly influence nanoparticle magnetization. Notably, our findings highlight pH 10 as optimal for magnetite nanoparticle synthesis, ensuring both purity and stability. Furthermore, our study elucidates the impact of pH on nanoparticle solubility and precipitation, crucial considerations for synthesis optimization. The development of magnetic nanomaterials with enhanced performance, as facilitated by this study, holds immense promise for biomedicine. By addressing factors influencing magnetization and synthesizing nanoparticles under optimized conditions, we advance the field, paving the way for improved applications in

magnetic hyperthermia and targeted drug delivery. In conclusion, the green synthesis of superparamagnetic magnetite nanoparticles using biological extracts presents a sustainable and effective approach with vast potential in biomedicine. Our study contributes valuable insights into synthesis optimization and nanoparticle characterization, driving innovation and progress in the development of magnetic nanomaterials for biomedical applications.

## Data availability statement

The original contributions presented in the study are included in the article/Supplementary Material, further inquiries can be directed to the corresponding author.

## Author contributions

MD: Formal Analysis, Investigation, Writing–original draft. BH-V: Methodology, Validation, Visualization, Writing–review and editing. PA: Funding acquisition, Project administration, Resources, Supervision, Visualization, Writing–review and editing.

## Conflict of interest

The authors declare that the research was conducted in the absence of any commercial or financial relationships that could be construed as a potential conflict of interest.

## Publisher's note

All claims expressed in this article are solely those of the authors and do not necessarily represent those of their affiliated organizations, or those of the publisher, the editors and the reviewers. Any product that may be evaluated in this article, or claim that may be made by its manufacturer, is not guaranteed or endorsed by the publisher.

# References

Akanda, M. R., Al-amin., M., Mele, M. A., Shuva, Z. M., Hossain, M. B., Islam, T., et al. (2023). Parameters optimization of Fe3O4 NPs synthesis by Tamarindus indica leaf extract possessing both peroxidase as well as excellent dye removal activity. *Heliyon* 9 (6), e16699. doi:10.1016/j.heliyon.2023.e16699

Akshay, V., Vasundhara, M., and Muthu, A. (2020). Biosynthesis of multiphase iron nanoparticles using Syzygium aromaticum and their magnetic properties. *Colloids Surf. A Physicochem. Eng. Aspect.* 603, 125241. doi:10.1016/j.colsurfa.2020.125241

Anastas, P. T., and Warner, J. C. (2000). *Green Chemistry: Theory and Practice*. Oxford: Oxford University Press.

Andrade, Â. L., Souza, D. M., Pereira, M. C., Fabris, J. D., and Domingues, R. Z. (2010). pH effect on the synthesis of magnetite nanoparticles by the chemical reduction-precipitation method. *Quím. Nova* 33, 524–527. doi:10.1590/S0100-40422010000300006

Andrade-Zavaleta, K., Chacon-Laiza, Y., Asmat-Campos, D., and Raquel-Checca, N. (2022). Green synthesis of superparamagnetic iron oxide nanoparticles with eucalyptus globulus extract and their application in the removal of heavy metals from agricultural soil. *Molecules* 27 (4), 1367. doi:10.3390/molecules27041367

Ashoori, F., Hajipour-Verdom, B., Satari, M., and Abdolmaleki, P. (2023). Polyethylenimine-based iron oxide nanoparticles enhance cisplatin toxicity in ovarian cancer cells in the presence of a static magnetic field. *Front. Oncol.* 13, 1217800. doi:10.3389/fonc.2023.1217800

Azizi, A. (2020). Green synthesis of Fe 3 O 4 nanoparticles and its application in preparation of Fe 3 O 4/cellulose magnetic nanocomposite: a suitable proposal for drug delivery systems. *J. Inorg. Organomet. Polym. Mater.* 30, 3552–3561. doi:10.1007/s10904-020-01500-1

Ba-Abbad, M. M., Benamour, A., Ewis, D., Mohammad, A. W., and Mahmoudi, E. (2022). Synthesis of Fe3O4 nanoparticles with different shapes through a co-precipitation method and their application. *JOM* 74 (9), 3531–3539. doi:10.1007/s11837-022-05380-3

Balintova, M., and Petrilakova, A. (2011). Study of pH influence on selective precipitation of heavy metals from acid mine drainage. *Chem. Eng. Trans.* 25, 345–350. doi:10.3303/CET1125058

Buazar, F., Baghlani-Nejazd, M. H., Badri, M., Kashisaz, M., Khaledi-Nasab, A., and Kroushawi, F. (2016). Facile one-pot phytosynthesis of magnetic nanoparticles using potato extract and their catalytic activity. *Starch-Stärke* 68 (7-8), 796–804. doi:10.1002/star.201500347

Campos, E. A., Stockler Pinto, D. V. B., Oliveira, J. I. S. d., Mattos, E. D. C., and Dutra, R. D. C. L. (2015). Synthesis, characterization and applications of iron oxide nanoparticles-a short review. *J. Aerosp. Technol. Manag.* 7, 267–276. doi:10.5028/jatm.v7i3.471

Chang, D., Lim, M., Goos, J. A. C. M., Qiao, R., Ng, Y. Y., Mansfeld, F. M., et al. (2018). Biologically targeted magnetic hyperthermia: potential and limitations. *Front. Pharmacol.* 9, 831. doi:10.3389/fphar.2018.00831

Chen, F., Ilyas, N., Liu, X., Li, Z., Yan, S., and Fu, H. (2021). Size effect of Fe3O4 nanoparticles on magnetism and dispersion stability of magnetic nanofluid. *Front. Energy Res.* 9, 780008. doi:10.3389/fenrg.2021.780008

Dehghani, M., and Ghadam, P. (2023). Green synthesis of ZnO-NPs by juglans regia green husk aqueous extract. *Mater. Proc.* 14 (1), 7. doi:10.3390/IOCN2023-14444

Dorniani, D., Kura, A. U., Ahmad, Z., Halim Shaari, A., Hussein, M. Z., and Fakurazi, S. (2012). Preparation of Fe₃O₄ magnetic nanoparticles coated with gallic acid for drug delivery. *Int. J. Nanomed.* 7, 5745–5756. doi:10.2147/IJN.S35746

DoymuŞ, K. (2007). The effect of ionic electrolytes and pH on the zeta potential of fine coal particles. *Turkish J. Chem.* 31 (6), 589–597. Available at: https://journals.tubitak.gov.tr/chem/vol31/iss6/3.

Ebrahimpour, A., Riahi Alam, N., Abdolmaleki, P., Hajipour-Verdom, B., Tirgar, F., Ebrahimi, T., et al. (2021). Magnetic metal–organic framework based on zinc and 5-aminolevulinic acid: MR imaging and brain tumor therapy. *J. Inorg. Organomet. Polym. Mater.* 31, 1208–1216. doi:10.1007/s10904-020-01782-5

Eldeeb, B. A., El-Raheem, W. M. A., and Elbeltagi, S. (2023). Green synthesis of biocompatible Fe3O4 magnetic nanoparticles using Citrus Sinensis peels extract for their biological activities and magnetic-hyperthermia applications. *Sci. Rep.* 13 (1), 19000. doi:10.1038/s41598-023-46287-6

Elizondo-Villarreal, N., Verástegui-Domínguez, L., Rodríguez-Batista, R., Gándara-Martínez, E., Alcorta-García, A., Martínez-Delgado, D., et al. (2022). Green synthesis of magnetic nanoparticles of iron oxide using aqueous extracts of lemon peel waste and its application in anti-corrosive coatings. *Materials* 15 (23), 8328. doi:10.3390/ma15238328

Etemadifar, R., Kianvash, A., Arsalani, N., Abouzari-Lotf, E., and Hajalilou, A. (2018). Green synthesis of superparamagnetic magnetite nanoparticles: effect of natural surfactant and heat treatment on the magnetic properties. *J. Mater. Sci. Mater. Electron.* 29, 17144–17153. doi:10.1007/s10854-018-9805-6

Fischer, U. A., Carle, R., and Kammerer, D. R. (2011). Identification and quantification of phenolic compounds from pomegranate (Punica granatum L.) peel, mesocarp, aril and differently produced juices by HPLC-DAD–ESI/MSn. *Food Chem.* 127 (2), 807–821. doi:10.1016/j.foodchem.2010.12.156

Ghasemi, R., Akrami Mohajeri, F., heydari, A., Yasini, S. A., Dehghani Tafti, A., and Khalili Sadrabad, E. (2023). Application of pomegranate peel extract, a waste agricultural product, as a natural preservative in tahini. *Int. J. Food Sci.* 2023, 1–7. doi:10.1155/2023/8860476

Hadadian, Y., Masoomi, H., Dinari, A., Ryu, C., Hwang, S., Kim, S., et al. (2022). From low to high saturation magnetization in magnetite nanoparticles: the crucial role of the molar ratios between the chemicals. *ACS Omega* 7 (18), 15996–16012. doi:10.1021/acsomega.2c01136

Hakami, O., Zhang, Y., and Banks, C. J. (2012). Thiol-functionalised mesoporous silica-coated magnetite nanoparticles for high efficiency removal and recovery of Hg from water. *Water Res.* 46 (12), 3913–3922. doi:10.1016/j.watres.2012.04.032

Harris, R. K., Becker, E. D., Cabral de Menezes, S. M., Goodfellow, R., and Granger, P. (2002). NMR nomenclature: nuclear spin properties and conventions for chemical shifts. IUPAC recommendations 2001. International union of pure and applied chemistry. Physical chemistry division. Commission on molecular structure and spectroscopy. *Magnetic Reson. Chem.* 40 (7), 489–505. doi:10.1006/snmr.2002.0063

Huang, X., and El-Sayed, M. A. (2010). Gold nanoparticles: optical properties and implementations in cancer diagnosis and photothermal therapy. *J. Adv. Res.* 1 (1), 13–28. doi:10.1016/j.jare.2010.02.002

Islam, K., Haque, M., Kumar, A., Hoq, A., Hyder, F., and Hoque, S. M. (2020). Manganese ferrite nanoparticles (MnFe2O4): size dependence for hyperthermia and negative/positive contrast enhancement in MRI. *Nanomaterials* 10 (11), 2297. doi:10.3390/nano10112297

Jana, J., Ganguly, M., and Pal, T. (2016). Enlightening surface plasmon resonance effect of metal nanoparticles for practical spectroscopic application. *RSC Adv.* 6 (89), 86174–86211. doi:10.1039/C6RA14173K

Kazemi-Ashtiyani, M., Hajipour-Verdom, B., Satari, M., Abdolmaleki, P., Hosseinkhani, S., and Shaki, H. (2022). Estimating the two graph dextran–stearic acid–spermine polymers based on iron oxide nanoparticles as carrier for gene delivery. *Biopolymers* 113 (7), e23491. doi:10.1002/bip.23491

Khairul, M., Shah, K., Doroodchi, E., Azizian, R., and Moghtaderi, B. (2016). Effects of surfactant on stability and thermo-physical properties of metal oxide nanofluids. *Int. J. Heat Mass Transf.* 98, 778–787. doi:10.1016/j.ijheatmasstransfer.2016.03.079

Khan, I., Saeed, K., and Khan, I. (2019). Nanoparticles: properties, applications and toxicities. *Arabian J. Chem.* 12 (7), 908–931. doi:10.1016/j.arabjc.2017.05.011

Kirby, B. J., and Hasselbrink, E. F., Jr (2004). Zeta potential of microfluidic substrates: 1. Theory, experimental techniques, and effects on separations. *Electrophoresis* 25 (2), 187–202. doi:10.1002/elps.200305754

Kiwumulo, H. F., Muwonge, H., Ibingira, C., Lubwama, M., Kirabira, J. B., and Ssekitoleko, R. T. (2022). Green synthesis and characterization of iron-oxide nanoparticles using Moringa oleifera: a potential protocol for use in low and middle income countries. *BMC Res. Notes* 15 (1), 149–158. doi:10.1186/s13104-022-06039-7

Kolen'ko, Y. V., Bañobre-López, M., Rodríguez-Abreu, C., Carbó-Argibay, E., Sailsman, A., Piñeiro-Redondo, Y., et al. (2014). Large-scale synthesis of colloidal Fe3O4 nanoparticles exhibiting high heating efficiency in magnetic hyperthermia. *J. Phys. Chem. C* 118 (16), 8691–8701. doi:10.1021/jp500816u

Kumar, B., Smita, K., Cumbal, L., and Debut, A. (2014). Biogenic synthesis of iron oxide nanoparticles for 2-arylbenzimidazole fabrication. *J. Saudi Chem. Soc.* 18 (4), 364–369. doi:10.1016/j.jscs.2014.01.003

Laurent, S., Forge, D., Port, M., Roch, A., Robic, C., Vander Elst, L., et al. (2008). Magnetic iron oxide nanoparticles: synthesis, stabilization, vectorization, physicochemical characterizations, and biological applications. *Chem. Rev.* 108 (6), 2064–2110. doi:10.1021/cr068445e

Lim, N., Santos, G. N., Ubando, A., and Culaba, A. B. (2021). Nanotechnology in the Philippines: development of framework for technology adoption. *IOP Conference Series: Materials Science and Engineering* 1109 (1), 012031. doi:10.1088/1757-899X/1109/1/012031

Maguire, C. M., Rösslein, M., Wick, P., and Prina-Mello, A. (2018). Characterisation of particles in solution–a perspective on light scattering and comparative technologies. *Sci. Technol. Adv. Mater.* 19 (1), 732–745. doi:10.1080/14686996.2018.1517587

Matrajt, G., Borg, J., Raynal, P. I., Djouadi, Z., d'Hendecourt, L., Flynn, G., et al. (2004). FTIR and Raman analyses of the Tagish Lake meteorite: relationship with the aliphatic hydrocarbons observed in the diffuse interstellar medium. *Astron. Astrophy.* 416 (3), 983–990. doi:10.1051/0004-6361:20034526

Mazrouaa, A. M., Mohamed, M. G., and Fekry, M. (2019). Physical and magnetic properties of iron oxide nanoparticles with a different molar ratio of ferrous and ferric. *Egypt. J. Petrol.* 28 (2), 165–171. doi:10.1016/j.ejpe.2019.02.002

Medina-Zazueta, L., Miranda-Castro, F. C., Romo-Garcia, F., Martínez-Gil, M., Esparza-Ponce, H. E., Encinas-Basurto, D., et al. (2023). Development of sustainable magnetic biosorbent using aqueous leaf extract of vallesia glabra for methylene blue removal from wastewater. *Sustainability* 15 (5), 4586. doi:10.3390/su15054586

Mishra, D., Arora, R., Lahiri, S., Amritphale, S. S., and Chandra, N. (2014). Synthesis and characterization of iron oxide nanoparticles by solvothermal method. *Prot. Metals Phys. Chem. Surf.* 50, 628–631. doi:10.1134/S2070205114050128

Molaabasi, F., Sarparast, M., Shamsipur, M., Irannejad, L., Moosavi-Movahedi, A. A., Ravandi, A., et al. (2018). Shape-controlled synthesis of luminescent hemoglobin capped hollow porous platinum nanoclusters and their application to catalytic oxygen reduction and cancer imaging. *Sci. Rep.* 8 (1), 14507. doi:10.1038/s41598-018-32918-w

Mubayi, A., Chatterji, S., Rai, P., and Watal, G. (2012). Evidence based green synthesis of nanoparticles. *Adv. Mater. Lett.* 3 (6), 519–525. doi:10.5185/amlett.2012.icnano.353

Mustapha, T., Misni, N., Ithnin, N. R., Daskum, A. M., and Unyah, N. Z. (2022). A review on plants and microorganisms mediated synthesis of silver nanoparticles, role of plants metabolites and applications. *Int. J. Environ. Res. Public Health* 19 (2), 674. doi:10.3390/ijerph19020674

Nandiyanto, A., and Al Husaeni, D. F. (2016). A bibliometric analysis of materials research in Indonesian journal using VOSviewer. *Indonesian J. Sci. Technol.* 1 (2), 132–155. doi:10.36909/jer.ASSEEE.16037

Nguyen, D. T., and Kim, K. S. (2016). Controlled synthesis of monodisperse magnetite nanoparticles for hyperthermia-based treatments. *Powder Technol.* 301, 1112–1118. doi:10.1016/j.powtec.2016.07.052

Nkurikiyimfura, I., Wang, Y., Safari, B., and Nshingabigwi, E. (2020). Temperature-dependent magnetic properties of magnetite nanoparticles synthesized via coprecipitation method. *J. Alloys Compd.* 846, 156344. doi:10.1016/j.jallcom.2020.156344

Rajan, A., and Sahu, N. K. (2020). Review on magnetic nanoparticle-mediated hyperthermia for cancer therapy. *J. Nanoparticle Res.* 22, 319–325. doi:10.1007/s11051-020-05045-9

Ramesh, P., Kokila, T., and Geetha, D. (2015). Plant mediated green synthesis and antibacterial activity of silver nanoparticles using Emblica officinalis fruit extract. *Spectrochimica Acta Part A Mol. Biomol. Spectrosc.* 142, 339–343. doi:10.1016/j.saa.2015.01.062

Sathishkumar, G., Logeshwaran, V., Sarathbabu, S., Jha, P. K., Jeyaraj, M., Rajkuberan, C., et al. (2018). Green synthesis of magnetic Fe3O4 nanoparticles using Couroupita guianensis Aubl. fruit extract for their antibacterial and cytotoxicity activities. *Artif. Cells Nanomed. Biotechnol.* 46 (3), 589–598. doi:10.1080/21691401.2017.1332635

Sengupta, A., and Sarkar, C. K. (2015). *Introduction to Nano: Basics to Nanoscience and Nanotechnology.* Berlin: Springer. doi:10.1007/978-3-662-47314-6

Shabatina, T. I., Vernaya, O. I., Shabatin, V. P., and Melnikov, M. Y. (2020). Magnetic nanoparticles for biomedical purposes: modern trends and prospects. *Magnetochemistry* 6 (3), 30. doi:10.3390/magnetochemistry6030030

Shamsipur, M., Chabok, A., Molaabasi, F., Seyfoori, A., Hajipour-Verdom, B., Shojaedin-Givi, B., et al. (2019). Label free phosphate functionalized semiconducting polymer dots for detection of iron (III) and cytochrome c with application to apoptosis imaging. *Biosens. Bioelectron.* 141, 111337. doi:10.1016/j.bios.2019.111337

Silva, V., Andrade, P., Silva, M., Bustamante D., A., De Los Santos Valladares, L., and Albino Aguiar, J. (2013). Synthesis and characterization of Fe3O4 nanoparticles coated with fucan polysaccharides. *J. Magnetism Magnetic Mater.* 343, 138–143. doi:10.1016/j.jmmm.2013.04.062

Skandalis, N., Dimopoulou, A., Georgopoulou, A., Gallios, N., Papadopoulos, D., Tsipas, D., et al. (2017). The effect of silver nanoparticles size, produced using plant extract from Arbutus unedo, on their antibacterial efficacy. *Nanomaterials* 7 (7), 178. doi:10.3390/nano7070178

Trivedi, M., Patil, S., Shettigar, H., Bairwa, K., and Jana, S. (2015). Spectroscopic characterization of biofield treated metronidazole and tinidazole. *Med. Chem.* 7 (5), 340–344. doi:10.4172/2161-0444.1000283

Venkataraman, S. (2022). Plant molecular pharming and plant-derived compounds towards generation of vaccines and therapeutics against coronaviruses. *Vaccines* 10 (11), 1805. doi:10.3390/vaccines10111805

Xu, C., and Sun, S. (2009). Superparamagnetic nanoparticles as targeted probes for diagnostic and therapeutic applications. *Dalton Trans.* (29), 5583–5591. doi:10.1039/b900272n

Yusefi, M., Shameli, K., Su Yee, O., Teow, S. Y., Hedayatnasab, Z., Jahangirian, H., et al. (2021). Green synthesis of Fe3O4 nanoparticles stabilized by a Garcinia mangostana fruit peel extract for hyperthermia and anticancer activities. *Int. J. Nanomed.* 16, 2515–2532. doi:10.2147/IJN.S284134

Zare-Moghadam, M., Shamsipur, M., Molaabasi, F., and Hajipour-Verdom, B. (2020). Chromium speciation by isophthalic acid-doped polymer dots as sensitive and selective fluorescent probes. *Talanta* 209, 120521. doi:10.1016/j.talanta.2019.120521